



Cite this: *Dalton Trans.*, 2025, **54**, 1655

Mechanism and optimization of ruthenium-catalyzed oxalamide synthesis using DFT[†]

Roger Monreal-Corona, Nicolas Joly, Sylvain Gaillard, Jean-Luc Renaud, Marc Valero,^a Enric Mayolas,^a Anna Pla-Quintana ^{*a} and Albert Poater ^{*a}

The oxalamide skeleton is a common structural motif in many biologically active molecules. These scaffolds can be synthesized via ruthenium pincer complex-catalyzed acceptorless dehydrogenative coupling of ethylene glycol and amines. In this study, we elucidate the mechanism of this oxalamide synthesis using density functional theory calculations. The rate-determining state is identified as the formation of molecular hydrogen following the oxidation of hydroxyacetamide to oxoacetamide. In predictive catalysis exercises, various modifications to the ruthenium pincer catalyst were investigated to assess their impact on the reactivity.

Received 13th November 2024,
Accepted 5th December 2024

DOI: 10.1039/d4dt03182b

rsc.li/dalton

1. Introduction

Among the most prevalent skeletons found in biologically active molecules are the oxalamide scaffolds (see Scheme 1). They are used in a variety of different drugs showing anti-coagulant activity¹ and also as inhibitors to the CD4-binding site of HIV-1,² as well as synthons for organosilica nanoparticles.³ Other uses include their presence in foods as flavouring agents.⁴ In the field of organometallic chemistry, they are used in cross-coupling reactions as robust ligands.⁵ Due to their importance, many different protocols have been developed for their efficient synthesis in recent years.

The most traditional methodology for the preparation of oxalamides involves the formation of acid chloride from oxalic acid and its further reaction with amines.^{5,6} Other strategies include the use of carbon monoxide for the oxidative carbonylation of amines or the aminolysis of oxalates,^{7,8} and more recently the reaction of dichloroacetamides and amines,⁹ but all these mentioned methodologies generate stoichiometric amounts of waste, use toxic reagents and are not atom economical. Consequently, the goal has been set to develop

new sustainable strategies that follow the green chemistry principles to be further implemented in the pharmaceutical sector.

In 2007, Milstein and coworkers reported a ruthenium-catalysed dehydrogenative coupling of alcohols with amines,¹⁰ resulting in the environmentally friendly synthesis of amides with H₂ as the only byproduct.¹¹ This acceptorless dehydrogenative coupling (ADC) reaction has been computationally studied by Milstein, Poater and collaborators.¹² Later, Milstein's and Guan's group¹³ demonstrated that a ruthenium pincer complex could also catalyse dehydrogenative coupling of diols and diamines to form polyamides.¹⁴ Other Ru-catalysed systems for synthesizing amides from amines and alcohols were subsequently developed.¹⁵ More recently, Milstein, Prakash and Liu groups¹⁶ have developed several liquid organic hydrogen carrier systems based on amide bond formation and reverse hydrogenation reactions.¹⁷ This amide formation has also been extended to the synthesis of primary amides from alcohols and ammonia.¹⁸ Knowing in advance that amines are a crucial group of compounds extensively utilized in agrochemicals, pharmaceuticals, and organic synthesis,¹⁹ several groups demonstrated that the resulting amides can be hydrogenated to regenerate these important amines.²⁰ This represents one of the greenest and most direct pathways for obtaining amines from feedstock compounds.

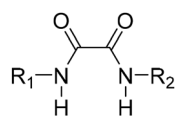
^aInstitut de Química Computacional i Catàlisi and Departament de Química, Universitat de Girona, c/Maria Àurelia Capmany 69, 17003 Girona, Catalonia, Spain. E-mail: anna.plaq@udg.edu, albert.poater@udg.edu

^bNormandie Univ., LCMT, ENSICAEN, UNICAEN, CNRS, 6 boulevard du Maréchal Juin, 14000 Caen, France. E-mail: jean-luc.renaud@sorbonne-universite.fr

^cSorbonne Université, CNRS, Institut Parisien de Chimie Moléculaire, UMR 8232, 75005 Paris, France

[†] Electronic supplementary information (ESI) available. See DOI: <https://doi.org/10.1039/d4dt03182b>

[‡]These authors contributed equally to this work.



Scheme 1 General structure of oxalamides.

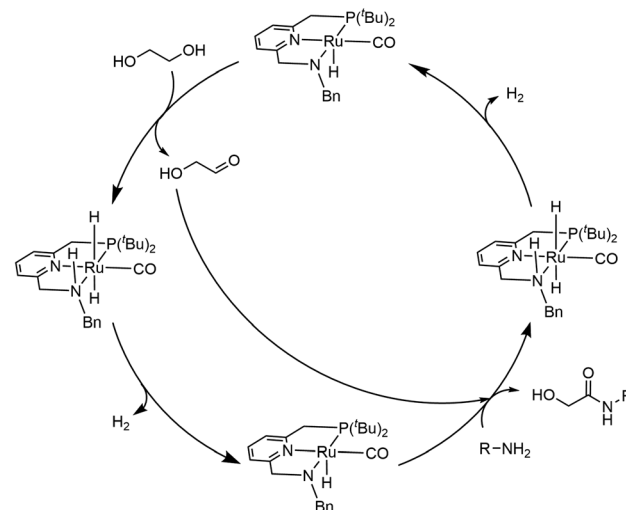


Ethylene glycol (EG) is a very convenient feedstock in industry since it is cheap, and it can be obtained from renewable biomass-derived hydrocarbons.^{21,22} Recently, Milstein and co-workers reported the use of the mentioned diol as an efficient hydrogen carrier, being able to load and unload hydrogen catalytically. In detail, EG is converted to oligoesters through acceptorless dehydrogenative esterification, and then these oligoesters are hydrogenated back to EG using a ruthenium pincer catalyst.

In 2020, Milstein and coworkers reported the ADC of ethylene glycol and amines for the atom-economical and sustainable synthesis of oxalamides.²³ Moreover, the known ability of oxalamides to act as chelating agents and cause product inhibition was overcome.²³ The reaction was performed in a single step by reacting EG with the desired amine, catalysed by a ruthenium pincer catalyst in the presence of ^tBuOK in toluene, at 135 °C for 24 hours (see Scheme 2).

Activation of the pre-catalyst into an unsaturated amidohydrido ruthenium complex *via* a basic treatment was initially postulated by Milstein. Coordination followed by a dehydrogenation step of EG could furnish the corresponding aldehyde (*i.e.* 2-hydroxy-ethanal) and the dihydrido-ruthenium pincer complex.²⁴ The latter, after hydrogen release, could regenerate the unsaturated ruthenium complex species, while the aldehyde could react with the amine to form a hemiaminal intermediate. A second dehydrogenation of the hemiaminal catalysed by the PNN ruthenium-pincer complex would furnish the hydroxyl-ethanamide and the dihydrido-ruthenium complex intermediate. A second catalytic cycle, after release of hydrogen, would allow the oxidation of the second alcohol and lead to the oxalamide compound (see Scheme 3). A deeper understanding of the process is however fundamental to understand the conversion of amines into amides. This process, using a ruthenium catalyst, is one of the few reported examples of oxalamide synthesis and reverse hydrogenation.⁸ Notably, a significant step was made towards the development of milder conditions for converting oxalamides back into amines and EG, achieving yields of up to 99%, with a reduction in temperature from 160 to 135 °C and a decrease in H₂ pressure from 60 to 40 atm.

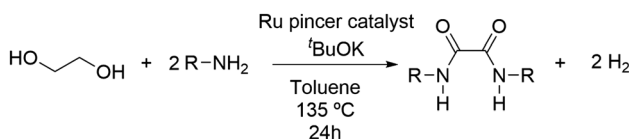
In this work, we aim to unveil the reaction mechanism for the formation of oxalamide scaffolds reported by Milstein and coworkers,²³ and, by predictive catalysis,²⁵ make use of computational tools to predict the modifications in both reactants and catalyst to lower the working temperature and improve the reported transformation.



Scheme 3 Proposed reaction mechanism for the reaction of ethylene glycol and primary amines for the synthesis of oxalamide scaffolds catalyzed by a ruthenium pincer catalyst.

2. Computational details

DFT calculations were performed with the Gaussian16 software package.²⁶ The BP86 functional of Becke and Perdew²⁷ was used to optimize the geometries, together with the Grimme D3 correction term for the electronic energy.^{28,29} The electronic configuration of the molecular systems was described with the SDD basis set and pseudopotential for ruthenium,³⁰ and the split-valence basis set with polarization functions of Ahlrichs and co-workers (Def2-SVP) for the rest of atoms.³¹ Frequency calculations were performed to ensure the nature located stationary points. In addition, the intrinsic reaction coordinate (IRC) procedure was used to confirm the two minima connected by each transition state.³² Implicit solvent effects were included to simulate toluene by means of the polarizable continuum model (PCM).³³ To improve accuracy, single point energy calculations with the M06 functional³⁴ and the Def2-TZVP basis set were carried out,³⁵ together with the Grimme D3 correction. These results yield energy barrier values within 2 kcal mol⁻¹ of those obtained from DLPNO-CCSD(T) calculations³⁶ by ORCA³⁷ demonstrating close agreement between the two computational approaches. The reported Gibbs energies include electronic energies computed at the M06-D3(PCM = toluene)/Def2-TZVP~SDD//BP86-D3/Def2-SVP~SDD corrected with zero-point energies, thermal corrections, and entropy effects evaluated with the BP86-D3/Def2-SVP~SDD method at 403.15 K and 1 atm.



Scheme 2 Reaction of ethylene glycol and primary amines for the synthesis of oxalamide scaffolds catalyzed by a ruthenium pincer catalyst.

3. Results and discussion

To gain insight into the reaction mechanism for the synthesis of oxalamides by acceptorless dehydrogenative coupling of ethylene glycol and amines catalyzed by ruthenium,²³ the reac-



tion profile was computed and is displayed in Fig. 2. The split mechanism is displayed in Fig. S1–S6.†

The reaction initiates from precatalytic species **A0** which is 3.1 kcal mol⁻¹ higher in energy than the catalytically active species **A**. Upon addition of ¹BuOK in the reaction mixture, the N–H bond of the side arm of the pincer ligand is activated through **TS-A0A** with a kinetic cost of 2.7 kcal mol⁻¹ in which ¹BuOH and KCl are formed, and **A** is generated *in situ*. With the catalytically active species in the reaction media, an ethylene glycol molecule is able to coordinate to the catalyst to form adduct **B** that evolves into the formation of experimentally detected species **C** after overcoming **TS-BC** with a kinetic cost of 6.6 kcal mol⁻¹. A second hydrogen atom is abstracted through **TS-CD** with an energy barrier of 15.4 kcal mol⁻¹ to yield species **D**. The release of a free molecule of glycolaldehyde to provide **E** is an endergonic process, with a relative energy of 8.9 kcal mol⁻¹ compared to **A**. The latter can set free H₂ through **TS-EF**, which is the most energetically demanding step of the first catalytic cycle, with an activation energy of 27.0 kcal mol⁻¹ (see Fig. 2),^{38,39} followed by an endergonic process by 3.4 kcal mol⁻¹ from **F** (Fig. 2). At this point, the free generated glycolaldehyde can follow three different reaction paths being (a) the oxidation of glycolaldehyde to oxalaldehyde, (b) the metal-free coupling of glycolaldehyde with a primary amine to form an hemiaminal intermediate, or (c) a metal-catalyzed coupling of glycolaldehyde with a primary amine. Milstein and coworkers observed that when only one equivalent of amine is used under the optimal reaction conditions, a hydroxyacetamide is obtained. This provides evidence that the coupling of glycolaldehyde and the amine is kinetically favoured over the oxidation of glycolaldehyde to oxalaldehyde. The computed energy profiles show that the oxidative process (a) does not occur, even though the activation energy is lower for this process compared to the coupling; the energy minimum corresponding to oxalaldehyde **C1** after overcoming **TS-B1C1** (see Fig. S3†) could not be found. When comparing the non-metal and metal catalyzed coupling of glycolaldehyde with a primary amine, the first displays a kinetic cost of 43.3 kcal mol⁻¹ that can be reduced to 39.0 and 36.0 kcal mol⁻¹, when the proton transfer is assisted by a water and ethylene glycol molecule, respectively (see Fig. S3†). On the other hand, coordination of glycolaldehyde to metal species **A** to form adduct **G** is endergonic by 16.0 kcal mol⁻¹, and in the presence of the amine, the formation of the C–N bond takes place in a barrierless step to yield intermediate metal-bound alkoxyde **H** with a relative energy of 7.9 kcal mol⁻¹. The Lewis acid character of the Ru catalyst induces significant polarization of the carbonyl group, increasing the charge on the carbon atom from 0.45 to 0.48 a.u. upon coordination to the Ru center. This polarization, combined with the strong hydrogen-bonding capability of the nitrogen atom, facilitates a barrierless nucleophilic attack of the amine on the carbonyl carbon. The latter path displays the lowest energy demand among those discussed. The generated metal-bound alkoxyde **H** proceeds to the hemiaminal intermediate **I** with a kinetic cost of 17.7 kcal mol⁻¹. The ruthenium catalyst oxidized the

in situ generated hemiaminal to the amide through **TS-IJ** with a kinetic cost of 13.1 kcal mol⁻¹ to recover species **E**. Release of H₂ upon overcoming a barrier of 18.1 kcal mol⁻¹ regenerates the catalytically active species **A**.

The catalytic cycle can start over to convert the second hydroxyl moiety to the aldehyde intermediate with energy barriers of 13.5 and 32.8 kcal mol⁻¹ for oxidation and H₂ release, respectively. The coupling of the second hexylamine is once again a barrierless process. Then, the formation of the hemiaminal takes place through an endergonic process by 6.5 kcal mol⁻¹. Finally, to obtain the desired oxalamide product,⁴⁰ the simultaneous deprotonation to oxidize the alcohol to the ketone takes place through **TS-IJ** with a kinetic cost of 13.3 kcal mol⁻¹. The last hydrogen production has an energy barrier of 18.1 kcal mol⁻¹ to recover the active catalytic species **A**, with a relative energy of -12.7 kcal mol⁻¹.

In summary, the synthesis of oxalamides from ethylene glycol and amines proceeds through four concatenated reaction paths being (A) the oxidation of the alcohol moiety to an aldehyde, (B) generation of molecular hydrogen, and (C) addition of the amine to the carbonyl function to furnish the amide functional groups, and (D) a second generation of molecular hydrogen to regain the active catalytic species. The most energy demanding step is the generation of H₂ after the release of the 2-oxoacetamide intermediate, with an overall energy barrier of 32.8 kcal mol⁻¹. The optimized geometry of **TS-EF** is shown in Fig. 1.

With the detailed mechanism in hand, we studied the effect of electronic and steric changes on the pincer ruthenium catalyst by including modifications to the phosphine moiety, pyridine ring, and the substituents on the nitrogen atom assisting the hydrogen transfer during the reaction mechanism. Given that the transition state **TS-EF** corresponding to the rate-determining state (rds) does not involve organic reactants (amine and ethylene glycol), the modifications to those species were not considered.^{12b,41} To accomplish this, the activation energy for the rds was calculated for a series of derivatives as depicted in Fig. 3.

First, modification was made to the phosphine moiety. Results show that electron-donating groups (EDGs) present slightly lower activation energies compared to electron-withdrawing groups (EWGs). Indeed the incorporation of CF₃ substituents on the phosphine increases the activation energy up

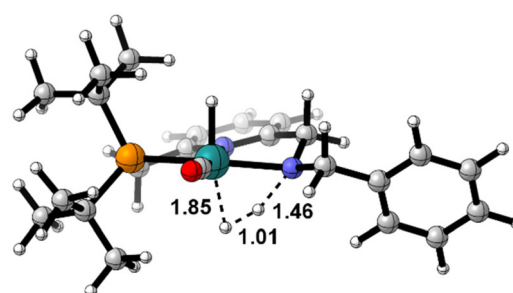


Fig. 1 Transition state **TS-EF**; selected distances in Å.

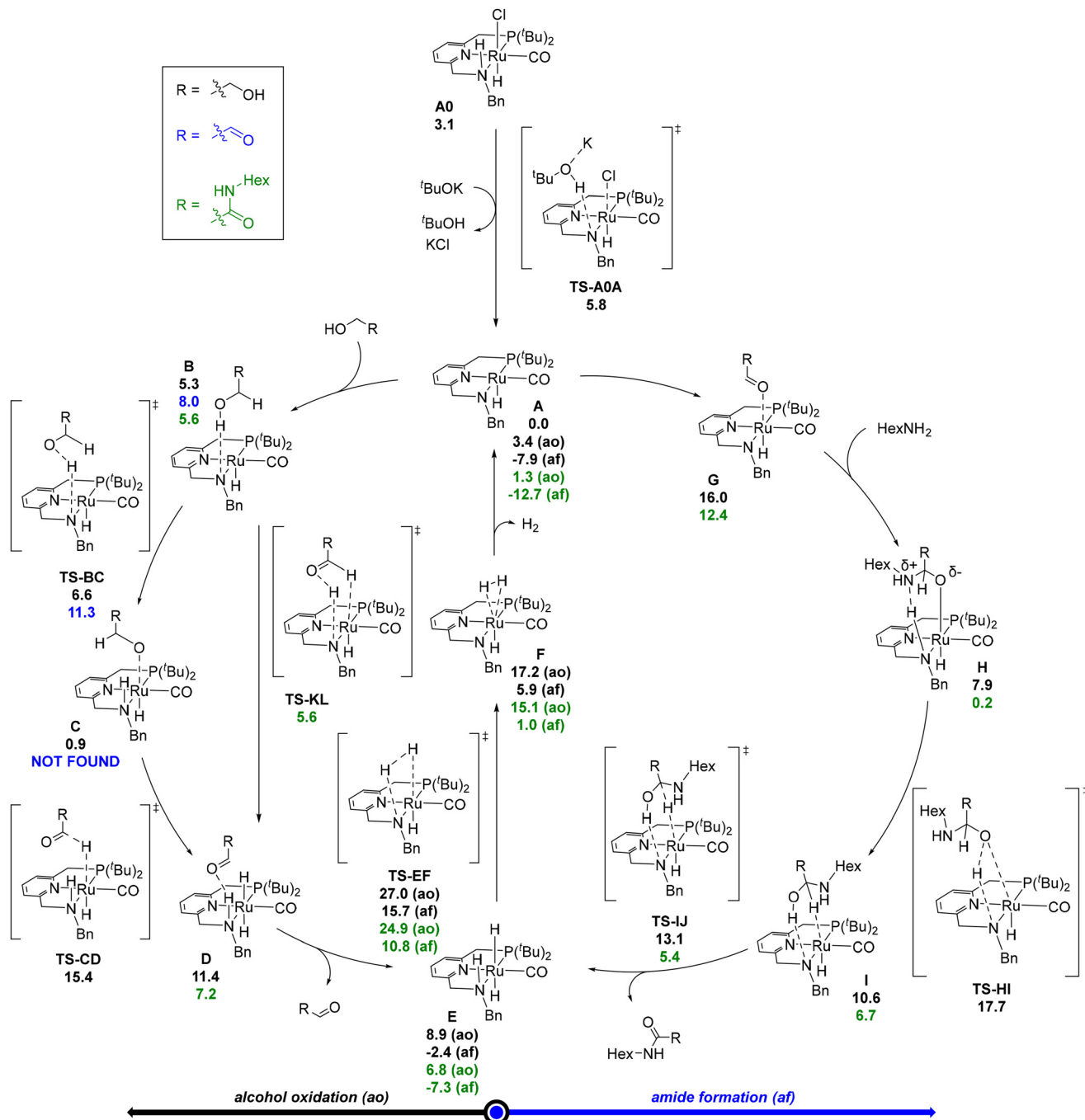


Fig. 2 Full reaction mechanism calculated at the M06-D3/Def2-TZVP-SDD_pcm-toluene//BP86-D3/Def2-SVP-SDD level of theory leading to the formation of oxalamides catalysed by a ruthenium pincer catalyst. Relative Gibbs energies in kcal mol⁻¹.

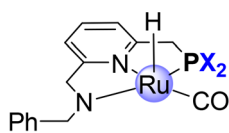
to 35.2 kcal mol⁻¹. Among the EDGs, activation energies range from 30.6 to 34.3 kcal mol⁻¹ for *t*Bu, *i*Pr, methyl, and methoxy substituents. Given the similarities in kinetic cost, we can draw the conclusion that steric effects are not important in the phosphine ligand, probably due to the large distance to the labile N–H bond, involved in the formation of molecular hydrogen.

Then, modifications were introduced at the *para* position of the pyridine ring. In this case, the effect is opposite to that

described before for the phosphines. Even though the changes in the activation energy are very subtle, the introduction of a fluorine or a trifluoromethyl substituent (EWG) reduces the kinetic cost to 32.5 kcal mol⁻¹ and 31.7 kcal mol⁻¹, respectively, whereas the presence of a methoxy group (EDG) increases the activation energy to 34.1 kcal mol⁻¹.

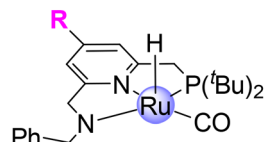
Finally, the nature of the environment around the labile N–H bond of the ligand was tuned. A series of (PNN)-ruthenium-pincer complexes has been already reported, and their appli-

Phosphine substituted derivatives:



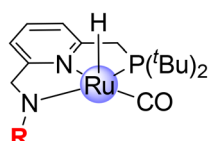
X =	<i>i</i> Pr, 30.6
	<i>t</i> Bu, 32.8
	CH ₃ , 34.2
	H, 34.3
	OCH ₃ , 34.3
	CF ₃ , 35.2

Pyridine substituted derivatives:



R =	CF ₃ , 31.7
	F, 32.5
	H, 32.8
	OCH ₃ , 34.1

Nitrogen substituted derivatives:



R =	<i>t</i> Bu, 29.5
	CH ₂ PhOCH ₃ , 29.7
	CH ₃ , 31.0
	CH ₂ OCH ₃ , 31.0
	Et, 31.9
	CH ₂ PhF, 32.7
	Bz, 32.8
	CH ₂ CF ₃ , 33.0
	CF ₃ , 34.9

Fig. 3 Pincer ruthenium catalyst derivatives and the activation energy (in kcal mol⁻¹) of the rds.

cation led to oxalamide derivatives in 26–96% yield.²³ The lowest yield was obtained with a PNN(Et)₂⁴² ligand showing that either the steric hindrance or the absence of NH function could impede the catalytic activity. Substitution of the benzyl substituent on the N atom by the bulky and EDG *t*Bu group resulted in a decrease to 29.5 kcal mol⁻¹, which was tested experimentally providing a yield of 37%, and therefore, indicating that other steps are hampered due to the introduction of a *t*Bu substituent. Other EDG groups, including *para*-substituted benzyl moieties resulted in barriers in the 29.7–32.7 kcal mol⁻¹ range. On the other hand, the presence of EWGs increases the kinetic cost of the rds, increasing with the proximity of the electronegative atoms, reaching 34.9 kcal mol⁻¹ for the trifluoromethyl substituent directly attached to the N atom. It is clear that a sterically large group pushes the two hydrogen atoms together easing the formation of molecular H₂ (see Fig. 4), and therefore decreasing the activation energy.

Steric map calculations were performed for the *t*Bu and CF₃ substituents on the N atom and are displayed in Fig. 5. A clear difference can be seen if we focus on the NW quadrant, corresponding to the substituent being exchanged, the steric hindrance of *t*Bu being considerably larger than that of CF₃, with overall %V_{bur} values of 80.7 and 73.9, respectively.

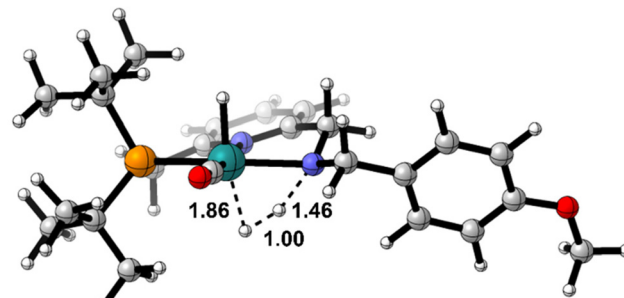
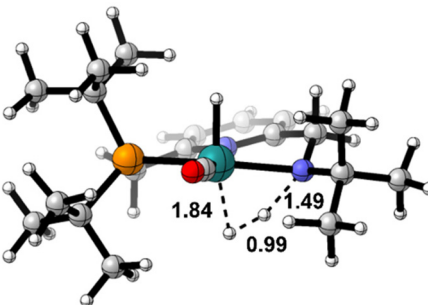


Fig. 4 Transition state TS-EF for catalyst derivatives bearing *t*Bu and CH₂PhOCH₃ substituents on the N atom; selected distances in Å.

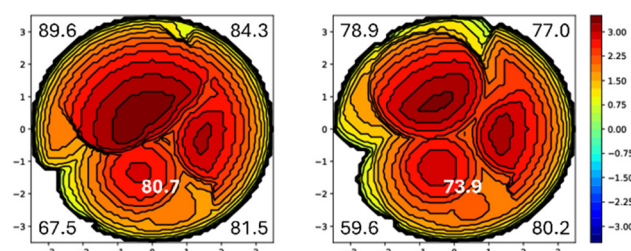


Fig. 5 Steric maps of species A for catalyst derivatives with *t*Bu (left) and CF₃ (right) substituents on the N atom, with the total %V_{bur} in white and by quadrants in black. The isocontour curves of the steric maps are in Å. The xz plane is the mean plane of the pincer ring, whereas the xz plane is the plane orthogonal to the mean plane of the NHC ring and passing through the carbene Ru atom.

Given that Milstein *et al.* tested experimentally Ru-PNN catalysts in which the side arm of the pincer consists of a C–H labile bond instead of an N–H bond, we computed the activation energy of the rds for two catalysts (see Fig. S7†). The results show higher energy barriers for catalysts **Ru-1** and **Ru-3** compared to those for catalyst **A**, with values of 38.5 and 34.7 kcal mol⁻¹, respectively. This is likely due to the greater energy required to activate a C–H bond compared to an N–H bond.⁴³ Additionally, the presence of a pyridine ring allows for better stabilization of the catalyst's aromatized/dearomatized forms, reducing the kinetic cost associated with the production of molecular hydrogen. Finally, the lability of the N–H bond facilitates significant alterations in the electronic environment around the nitrogen atom, thereby modulating the nature of the N–Ru interaction. This modulation likely con-

tributes to the acceleration of key steps in the reaction mechanism.

Experimentally, it is also essential to confirm that this beneficial substitution, in terms of economic and milder conditions, is achievable. It is also worth noting that scanning a selection of substrates did not indicate that their performance was due to either a kinetic or thermodynamic reformulation. At least, no correlation between yield and either of these two criteria was achieved (see the ESI†).

Moreover, looking further ahead, the study also examined the effects of modifying the nature of the metal, towards sustainability, with the aim of replacing ruthenium with iron, reducing the cost and toxicity because of the metal.⁴⁴ However, except for a few rare cases where iron is competitive with ruthenium,⁴⁵ such as with hydrogenating Knölker catalysts and its derivatives, most efforts have been limited to computational attempts⁴⁴ or experimental insights with low efficiency.⁴⁶ For the reference experimental system using ruthenium, replacing it with osmium worsened the results by only 0.8 kcal mol⁻¹, but switching to iron significantly reduced the energy by 3.2 kcal mol⁻¹. This reconfirms the necessity of having the two hydrogens as close as possible. This is a preliminary result, requiring not only experiments, but first more theoretical verification to ensure that the nature of the metal does not alter the rds and that the overall mechanism remains feasible.

4. Conclusions

In this study, we elucidate the catalytic cycle for the ruthenium pincer complex-catalysed synthesis of oxalamides from ethylene glycol and amines using DFT calculations. The reaction mechanism consists of the oxidation of glycolaldehyde to acetaldehyde, followed by the metal-catalysed coupling of the aldehyde with the primary amine to form the hydroxyacetamide intermediate. Then, the second oxidation and amine coupling take place following an identical reaction pathway. The rds of the transformation is identified as the formation of molecular hydrogen, following the oxidation of hydroxyacetamide to oxoacetamide. Various modifications were made to the ruthenium pincer catalyst to assess their impact on the catalytic reactivity. The results indicate that substitutions on the phosphine moiety, pyridine ligand, and nitrogen atom of the pincer ligand have minimal effect on the activation energy. It is important to note, however, that the latest modification, which involved the introduction of electron-donating groups with a greater steric effect, has led to more significant variations, reducing the kinetic cost of the rds. Consequently, even though the catalyst developed by Milstein *et al.* demonstrates optimal performance, experimental modifications to this catalyst are likely to reduce the kinetic barriers or enable milder reaction conditions. In general, not just for this particular reaction, but for the ADC to occur, it is necessary for the two hydrogens to come together to release H₂.

Author contributions

R. M.-C.: data curation, formal analysis, investigation, methodology, visualization, and writing – original draft. N. J.: data curation, formal analysis, and investigation. S. G.: formal analysis, investigation, supervision, validation, visualization, and review & editing. J. L.-R.: conceptualization, funding acquisition, methodology, project administration, supervision, validation, visualization, and review & editing. M. V.: data curation, formal analysis, and investigation. E. M.: data curation, formal analysis, and investigation. A. P.-Q.: conceptualization, funding acquisition, methodology, project administration, supervision, validation, visualization, and review & editing. A. P.: conceptualization, data curation, funding acquisition, methodology, project administration, supervision, visualization, writing – original draft, and review & editing.

Data availability

The data supporting the findings of this study are available within the article and its ESI.†

Conflicts of interest

There are no conflicts to declare.

Acknowledgements

A. P. and A. P.-Q. are Serra Húnter Fellows. A. P. received ICREA Academia Prize 2019. We thank the Ministerio de Economía y Competitividad (MINECO) for project PGC2018-097722-B-I00 (to A. P.) and Ministerio de Ciencia e Innovación for PID2020-113711GB-I00 MCIN/AEI/10.13039/501100011033 and PID2023-146849NB-I00 (to A. P.-Q.). We thank the Spanish Government for the predoctoral FPU20/00707 grant to R. M.-C. Financial support from the “Ministère de la Recherche et des Nouvelles Technologies”, Normandie Université, University of Caen Normandie, CNRS, “Région Normandie”, and the LABEX SynOrg (ANR-11-LABEX-0029) is acknowledged.

References

- 1 J. T. Njardarson, Poster: Top 200 Pharmaceutical Products by Retail Sales in 2018.
- 2 (a) F. Curreli, S. Choudhury, I. Pyatkin, V. P. Zagorodnikov, A. K. Bulay, A. Altieri, Y. D. Kwon, P. D. Kwong and A. K. Debnath, Design, synthesis, and antiviral activity of entry inhibitors that target the CD4-binding site of HIV-1, *J. Med. Chem.*, 2012, **55**, 4764–4775; (b) F. Curreli, Y. D. Kwon, H. Zhang, Y. Yang, D. Seacalossi, P. D. Kwong and A. K. Debnath, Binding mode characterization of NBD series CD4-mimetic HIV-1 entry inhibitors by X-ray struc-

ture and resistance study, *Antimicrob. Agents Chemother.*, 2014, **58**, 5478–5491.

3 (a) J. G. Croissant, Y. Fatieiev, K. Julfakyan, J. Lu, A. Emwas, D. H. Anjum, H. Omar, F. Tamanoi, J. I. Zink and N. M. Khashab, Biodegradable oxamide-phenylene-based mesoporous organosilica nanoparticles with unprecedented drug payloads for delivery in cells, *Chem. – Eur. J.*, 2016, **22**, 14806–14811; (b) Y. Fatieiev, J. G. Croissant, K. Julfakyan, L. Deng, D. H. Anjum, A. Gurinov and N. M. Khashab, Enzymatically degradable hybrid organic-inorganic bridged silsesquioxane nanoparticles for *in vitro* imaging, *Nanoscale*, 2015, **7**, 15046–15050.

4 K. Abdelmajid and W. Cornelis, WO 2011095533A1, 2011.

5 (a) Z. Chen, Y. Jiang, L. Zhang, Y. Guo and D. Ma, Oxalic diamides and *tert*-butoxide: two types of ligands enabling practical access to alkyl aryl ethers via Cu-catalyzed coupling reaction, *J. Am. Chem. Soc.*, 2019, **141**, 3541–3549; (b) W. Zhou, M. Fan, J. Yin, Y. Jiang and D. Ma, CuI/oxalic diamide catalyzed coupling reaction of (hetero)aryl chlorides and amines, *J. Am. Chem. Soc.*, 2015, **137**, 11942–11945; (c) S. De, J. Yin and D. Ma, Copper-catalyzed coupling reaction of (hetero)aryl chlorides and amides, *Org. Lett.*, 2017, **19**, 4864–4867; (d) M. Fan, W. Zhou, Y. Jiang and D. Ma, Assembly of primary (hetero)arylamines via CuI/oxalic diamide-catalyzed coupling of aryl chlorides and ammonia, *Org. Lett.*, 2015, **17**, 5934–5937; (e) G. Pawar, H. Wu, S. De and D. Ma, Copper(I) oxide/*N,N'*-Bis[(2-furyl)methyl]oxalamide-catalyzed coupling of (hetero)aryl halides and nitrogen heterocycles at low catalytic loading, *Adv. Synth. Catal.*, 2017, **359**, 1631–1636; (f) V. S. Chan, S. W. Krabbe, C. Li, L. Sun, Y. Liu and A. J. Nett, Identification of an oxalamide ligand for copper-catalyzed C–O couplings from a pharmaceutical compound library, *ChemCatChem*, 2019, **11**, 5748–5753; (g) D. V. Morarji and K. K. Gurjar, Theoretical and experimental studies: Cu(I)/Cu(II) catalytic cycle in CuI/oxalamide-promoted C–N bond formation, *Organometallics*, 2019, **38**, 2502–2511.

6 D. Ma, W. Zhou, M. Fan, H. Wu, J. Yin and S. Xia, US Pat., 20180207628A1, 2018.

7 (a) R. Mancuso, D. S. Raut, N. D. Ca', F. Fini, C. Cargagna and B. Gabriele, Catalytic oxidative carbonylation of amino moieties to ureas, oxamides, 2-oxazolidinones, and benzoxazolones, *ChemSusChem*, 2015, **8**, 2204–2211; (b) B. P. Woods, M. Orlandi, C.-Y. Huang, M. S. Sigman and A. G. Doyle, Nickel-catalyzed enantioselective reductive cross-coupling of styrenyl aziridines, *J. Am. Chem. Soc.*, 2017, **139**, 5688–5691; (c) S. Şeker, D. Barış, N. Arslan, Y. Turgut, N. Pirinçioğlu and M. Toğrul, Synthesis of rigid and C_2 -symmetric pyridino-15-crown-5 type macrocycles bearing diamide-diester functions: enantiomeric recognition for chiral primary organoammonium perchlorate salts, *Tetrahedron: Asymmetry*, 2014, **25**, 411–417.

8 K. Dong, S. Elangovan, R. Sang, A. Spannenberg, R. Jackstell, K. Junge, Y. Li and M. Beller, Selective catalytic two-step process for ethylene glycol from carbon monoxide, *Nat. Commun.*, 2016, **7**, 12075.

9 A. Jayaram, V. T. Seenivasan, K. Govindan, Y.-M. Liu, N.-Q. Chen, T.-W. Yeh, G. Venkatachalam, C.-H. Li, T.-F. Leung and W.-Y. Lin, Base-promoted triple cleavage of CCl_2Br : a direct one-pot synthesis of unsymmetrical oxalamide derivatives, *Chem. Commun.*, 2024, **60**, 3079–3082.

10 C. Gunanathan, Y. Ben-David and D. Milstein, Direct synthesis of amides from alcohols and amines with liberation of H_2 , *Science*, 2007, **317**, 790–792.

11 J. A. Luque-Urrutia, T. Ortiz-García, M. Solà and A. Poater, Green Energy by Hydrogen Production from Water Splitting, Water Oxidation Catalysis and Acceptorless Dehydrogenative Coupling, *Inorganics*, 2023, **11**, 88.

12 (a) J. A. Luque-Urrutia, M. Solà, D. Milstein and A. Poater, Mechanism of the Manganese-Pincer Catalyzed Acceptorless Dehydrogenative Coupling of Nitriles and Alcohols, *J. Am. Chem. Soc.*, 2019, **141**, 2398–2403; (b) J. Masdemont, J. A. Luque-Urrutia, M. Gimferrer, D. Milstein and A. Poater, Mechanism of Coupling of Alcohols and Amines to Generate Aldimines and H_2 by a Pincer Manganese Catalyst, *ACS Catal.*, 2019, **9**, 1662–1669; (c) A. Cicolella, M. C. D'Alterio, J. Duran, S. Simon, G. Talarico and A. Poater, Combining both Acceptorless Dehydrogenation and Borrowing Hydrogen Mechanisms in one System as described by DFT Calculations, *Adv. Theory Simul.*, 2022, **5**, 2100566.

13 H. Zeng and Z. Guan, Direct Synthesis of Polyamides via Catalytic Dehydrogenation of Diols and Diamines, *J. Am. Chem. Soc.*, 2011, **133**, 1159–1161.

14 B. Gnanaprakasam, E. Balaraman, C. Gunanathan and D. Milstein, Synthesis of Polyamides from Diols and Diamines with Liberation of H_2 , *J. Polym. Sci., Part A: Polym. Chem.*, 2012, **50**, 1755–1765.

15 (a) L. U. Nordström, H. Vogt and R. Madsen, Amide Synthesis from Alcohols and Amines by the Extrusion of Dihydrogen, *J. Am. Chem. Soc.*, 2008, **130**, 17672–17673; (b) A. J. A. Watson, A. C. Maxwell and J. M. J. Williams, Ruthenium-catalyzed oxidation of alcohols into amides, *Org. Lett.*, 2009, **11**, 2667–2670; (c) A. Prades, E. Peris and M. Albrecht, Organometallic hydrogen transfer and dehydrogenation catalysts for the conversion of bio-renewable alcohols, *Organometallics*, 2011, **30**, 1162–1167; (d) T. Zweifel, J.-V. Naubron and H. Grützmacher, Catalyzed dehydrogenative coupling of primary alcohols with water, methanol, or amines, *Angew. Chem., Int. Ed.*, 2009, **48**, 559–563; (e) S. C. Ghosh, S. Muthaiah, Y. Zhang, X. Xu and S. H. Hong, Direct Amide Synthesis from Alcohols and Amines by Phosphine-Free Ruthenium Catalyst Systems, *Adv. Synth. Catal.*, 2009, **351**, 2643–2649; (f) D. Srimani, E. Balaraman, P. Hu, Y. Ben-David and D. Milstein, Catalytic coupling of nitriles with amines to selectively form imines under mild hydrogen pressure, *Adv. Synth. Catal.*, 2013, **355**, 2525–2530.

16 (a) J. Kothandaraman, S. Kar, R. Sen, A. Goepert, G. Olah and G. K. S. Prakash, Efficient Reversible Hydrogen Carrier System Based on Amine Reforming of Methanol, *J. Am. Chem. Soc.*, 2017, **139**, 2549–2552; (b) Z. Shao, Y. Li, C. Liu,



W. Ai, S.-P. Luo and Q. Liu, Reversible interconversion between methanol-diamine and diamide for hydrogen storage based on manganese catalyzed (de)hydrogenation, *Nat. Commun.*, 2020, **11**, 591.

17 (a) P. Hu, E. Fogler, Y. Diskin-Posner, M. A. Iron and D. Milstein, A novel liquid organic hydrogen carrier system based on catalytic peptide formation and hydrogenation, *Nat. Commun.*, 2015, **6**, 6859; (b) P. Hu, Y. Ben-David and D. Milstein, Rechargeable Hydrogen Storage System Based on the Dehydrogenative Coupling of Ethylenediamine with Ethanol, *Angew. Chem., Int. Ed.*, 2016, **55**, 1061–1064; (c) A. Kumar, T. Janes, N. A. Espinosa-Jalapa and D. Milstein, Selective Hydrogenation of Cyclic Imides to Diols and Amines and Its Application in the Development of a Liquid Organic Hydrogen Carrier, *J. Am. Chem. Soc.*, 2018, **140**, 7453–7457; (d) Y. Xie, P. Hu, Y. Ben-David and D. Milstein, A Reversible Liquid Organic Hydrogen Carrier System Based on Methanol-Ethylenediamine and Ethylene Urea, *Angew. Chem., Int. Ed.*, 2019, **58**, 5105–5109.

18 J. Luo, Q.-Q. Zhou, M. Montag, Y. Ben-David and D. Milstein, Acceptorless dehydrogenative synthesis of primary amides from alcohols and ammonia, *Chem. Sci.*, 2022, **13**, 3894–3901.

19 (a) S. A. Lawrence, *Amines: Synthesis, Properties and Applications*, Cambridge University Press, Cambridge, 2004; (b) P. Roose, K. Eller, E. Henkes, R. Rossbacher and H. Höke, Amines, Aliphatic, in *Ullmann's Encyclopedia of Industrial Chemistry*, Wiley-VCH, Weinheim, 2015.

20 (a) N. Gorgas and K. Kirchner, Isoelectronic Manganese and Iron Hydrogenation/Dehydrogenation Catalysts: Similarities and Divergences, *Acc. Chem. Res.*, 2018, **51**, 1558–1569; (b) F. Kallmeier and R. Kempe, Manganese Complexes for (De)Hydrogenation Catalysis: A Comparison to Cobalt and Iron Catalysts, *Angew. Chem., Int. Ed.*, 2018, **57**, 46–60; (c) V. Papa, J. R. Cabrero-Antonino, E. Alberico, A. Spanneberg, K. Junge, H. Junge and M. Beller, Efficient and selective hydrogenation of amides to alcohols and amines using a well-defined manganese-PNN pincer complex, *Chem. Sci.*, 2017, **8**, 3576–3585; (d) E. Balaraman, B. Gnanaprakasam, L. J. W. Shimon and D. Milstein, Direct hydrogenation of amides to alcohols and amines under mild conditions, *J. Am. Chem. Soc.*, 2010, **132**, 16756–16758; (e) J. R. Cabrero-Antonino, E. Alberico, H. J. Drexler, W. Baumann, K. Junge, H. Junge and M. Beller, Efficient base-free hydrogenation of amides to alcohols and amines catalyzed by well-defined pincer imidazolyl-ruthenium complexes, *ACS Catal.*, 2016, **6**, 47–54; (f) N. M. Rezayee, D. C. Samblanet and M. S. Sanford, Iron-Catalyzed Hydrogenation of Amides to Alcohols and Amines, *ACS Catal.*, 2016, **6**, 6377–6383; (g) M. Ito, T. Ootsuka, R. Watari, A. Shiibashi, A. Himizu and T. Ikariya, Catalytic hydrogenation of carboxamides and esters by well-defined Cp^* Ru complexes bearing a protic amine ligand, *J. Am. Chem. Soc.*, 2011, **133**, 4240–4242; (h) J. M. John and S. H. Bergens, A Highly Active Catalyst for the Hydrogenation of Amides to Alcohols and Amines, *Angew. Chem., Int. Ed.*, 2011, **50**, 10377–10380.

21 H. Yue, Y. Zhao, X. Ma and J. Gong, Ethylene glycol: properties, synthesis, and applications, *Chem. Soc. Rev.*, 2012, **41**, 4218–4244.

22 A. Wang and T. Zhang, One-pot conversion of cellulose to ethylene glycol with multifunctional tungsten-based catalysts, *Acc. Chem. Res.*, 2013, **46**, 1377–1386.

23 Y.-Q. Zou, Q.-Q. Zhou, Y. Diskin-Posner, Y. Ben-David and D. Milstein, Synthesis of oxalamides by acceptorless dehydrogenative coupling of ethylene glycol and amines and the reverse hydrogenation catalyzed by ruthenium, *Chem. Sci.*, 2020, **11**, 7188–7193.

24 (a) H. Grützmacher, Cooperating Ligands in Catalysis, *Angew. Chem., Int. Ed.*, 2008, **47**, 1814–1818; (b) J. I. van der Vlugt and J. N. H. Reek, Neutral tridentate PNP ligands and their hybrid analogues: versatile non-innocent scaffolds for homogeneous catalysis, *Angew. Chem., Int. Ed.*, 2009, **48**, 8832–8846; (c) G. E. Dobereiner and R. H. Crabtree, Dehydrogenation as a substrate-activating strategy in homogeneous transition-metal catalysis, *Chem. Rev.*, 2010, **110**, 681–703; (d) J. R. Khusnutdinova and D. Milstein, Metal-ligand cooperation, *Angew. Chem., Int. Ed.*, 2015, **54**, 12236–12273; (e) K. Sordakis, C. Tang, L. Vogt, H. Junge, P. J. Dyson and M. Beller, Homogeneous Catalysis for Sustainable Hydrogen Storage in Formic Acid and Alcohols, *Chem. Rev.*, 2018, **118**, 372–433.

25 (a) S. Escayola, N. Bahri-Laleh and A. Poater, %V_{Bur} index and steric maps: from predictive catalysis to machine learning, *Chem. Soc. Rev.*, 2024, **53**, 853–882; (b) R. Monreal-Corona, A. Pla-Quintana and A. Poater, Predictive catalysis: a valuable step towards machine learning, *Trends Chem.*, 2023, **5**, 935–946; (c) M. Tomasini, M. Voccia, L. Caporaso, M. Szostak and A. Poater, Tuning the steric hindrance of alkylamines: a predictive model of steric editing of planar amines, *Chem. Sci.*, 2024, **15**, 13405–13414.

26 M. J. Frisch, G. W. Trucks, H. B. Schlegel, G. E. Scuseria, M. A. Robb, J. R. Cheeseman, G. Scalmani, V. Barone, G. A. Petersson, H. Nakatsuji, X. Li, M. Caricato, A. V. Marenich, J. Bloino, B. G. Janesko, R. Gomperts, B. Mennucci, H. P. Hratchian, J. V. Ortiz, A. F. Izmaylov, J. L. Sonnenberg, D. Williams-Young, F. Ding, F. Lipparini, F. Egidi, J. Goings, B. Peng, A. Petrone, T. Henderson, D. Ranasinghe, V. G. Zakrzewski, J. Gao, N. Rega, G. Zheng, W. Liang, M. Hada, M. Ehara, K. Toyota, R. Fukuda, J. Hasegawa, M. Ishida, T. Nakajima, Y. Honda, O. Kitao, H. Nakai, T. Vreven, K. Throssell, J. A. Montgomery Jr, J. E. Peralta, F. Ogliaro, M. J. Bearpark, J. J. Heyd, E. N. Brothers, K. N. Kudin, V. N. Staroverov, T. A. Keith, R. Kobayashi, J. Normand, K. Raghavachari, A. P. Rendell, J. C. Burant, S. S. Iyengar, J. Tomasi, M. Cossi, J. M. Millam, M. Klene, C. Adamo, R. Cammi, J. W. Ochterski, R. L. Martin, K. Morokuma, O. Farkas, J. B. Foresman and D. J. Fox, *Gaussian 16, Revision C.01*, Gaussian, Inc., Wallingford CT, 2016.

27 (a) A. Becke, Density-functional exchange-energy approximation with correct asymptotic behaviour, *Phys. Rev. A: At., Mol., Opt. Phys.*, 1988, **38**, 3098–3100; (b) J. P. Perdew, Density-functional approximation for the correlation energy of the inhomogeneous electron gas, *Phys. Rev. B: Condens. Matter Mater. Phys.*, 1986, **33**, 8822–8824; (c) J. P. Perdew, Erratum: Density-functional approximation for the correlation energy of the inhomogeneous electron gas, *Phys. Rev. B: Condens. Matter Mater. Phys.*, 1986, **34**, 7406–7406.

28 S. Grimme, J. Antony, S. Ehrlich and H. Krieg, A consistent and accurate ab initio parametrization of density functional dispersion correction (DFT-D) for the 94 elements H–Pu, *J. Chem. Phys.*, 2010, **132**, 154104.

29 S. Grimme, S. Ehrlich and L. Goerigk, Effect of the damping function in dispersion corrected density functional theory, *J. Comput. Chem.*, 2011, **32**, 1456–1465.

30 (a) U. Häussermann, M. Dolg, H. Stoll, H. Preuss, P. Schwerdtfeger and R. Pitzer, Accuracy of energy-adjusted quasirelativistic ab initio pseudopotentials: all-electron and pseudopotential benchmark calculations for Hg, HgH and their cations, *Mol. Phys.*, 1993, **78**, 1211–1224; (b) W. Küchle, M. Dolg, H. Stoll and H. Preuss, Energy-adjusted pseudopotentials for the actinides. Parameter sets and test calculations for thorium and thorium monoxide, *J. Chem. Phys.*, 1994, **100**, 7535–7542; (c) T. Leininger, A. Nicklass, H. Stoll, M. Dolg and P. Schwerdtfeger, The accuracy of the pseudopotential approximation. II. A comparison of various core sizes for indium pseudopotentials in calculations for spectroscopic constants of InH, InF, and InCl, *J. Chem. Phys.*, 1996, **105**, 1052–1059.

31 A. Schäfer, H. Horn and R. Ahlrichs, Fully optimized contracted Gaussian basis sets for atoms Li to Kr, *J. Chem. Phys.*, 1992, **97**, 2571–2577.

32 C. Gonzalez and H. B. Schlegel, An improved algorithm for reaction path following, *J. Chem. Phys.*, 1989, **90**, 2154–2161.

33 V. Barone, M. Cossi and J. Tomasi, A new definition of cavities for the computation of solvation free energies by the polarizable continuum model, *J. Chem. Phys.*, 1997, **107**, 3210–3221.

34 Y. Zhao and D. G. Truhlar, The M06 suite of density functionals for main group thermochemistry, thermochemical kinetics, noncovalent interactions, excited states, and transition elements: Two new functionals and systematic testing of four M06-class functionals and 12 other functionals, *Theor. Chem. Acc.*, 2008, **120**, 1–3.

35 (a) F. Weigend and R. Ahlrichs, Balanced basis sets of split valence, triple zeta valence and quadruple zeta valence quality for H to Rn: Design and assessment of accuracy, *Phys. Chem. Chem. Phys.*, 2005, **7**, 3297–3305; (b) R. Krishnan, J. S. Binkley, R. Seeger and J. A. Pople, Self-consistent molecular orbital methods. XX. A basis set for correlated wave functions, *J. Chem. Phys.*, 1980, **72**, 650–654.

36 C. Riplinger and F. Neese, An efficient and near linear scaling pair natural orbital based local coupled cluster method, *J. Chem. Phys.*, 2013, **138**, 034106.

37 F. Neese, The ORCA program system, *Wiley Interdiscip. Rev.: Comput. Mol. Sci.*, 2012, **2**, 73–78.

38 H. Li, X. Wang, F. Huang, G. Lu, J. Jiang and Z.-X. Wang, Computational Study on the Catalytic Role of Pincer Ruthenium(II)-PNN Complex in Directly Synthesizing Amide from Alcohol and Amine: The Origin of Selectivity of Amide over Ester and Imine, *Organometallics*, 2011, **30**, 5233–5247.

39 O. Blum and D. Milstein, Mechanism of a directly observed. β -hydride elimination process of iridium alkoxo complexes, *J. Organomet. Chem.*, 2000, **593–594**, 479–484.

40 M. Montag and D. Milstein, Sustainable amidation through acceptorless dehydrogenative coupling by pincer-type catalysts: recent advances, *Pure Appl. Chem.*, 2023, **95**, 109–124.

41 M. Gimferrer, M. C. D'Alterio, G. Talarico, Y. Minami, T. Hiyama and A. Poater, Allyl Monitorization of the Regioselective Pd-Catalyzed Annulation of Alkynyl Aryl Ethers Leading to Bismethylenechromanes, *J. Org. Chem.*, 2020, **85**, 12262–12269.

42 J. Zhang, G. Leitus, Y. Ben-David and D. Milstein, Facile Conversion of Alcohols into Esters and Dihydrogen Catalyzed by New Ruthenium Complexes, *J. Am. Chem. Soc.*, 2005, **127**, 10840–10841.

43 (a) T. He, J. C. Buttner, E. F. Reynolds, J. Pham, J. C. Malek, J. M. Keith and A. R. Chianese, Dehydroalkylative Activation of CNN- and PNN-Pincer Ruthenium Catalysts for Ester Hydrogenation, *J. Am. Chem. Soc.*, 2019, **141**, 17404–17413; (b) J. Pham, C. E. Jarczyk, E. F. Reynolds, S. E. Kelly, T. Kim, T. He, J. M. Keith and A. R. Chianese, The key role of the latent N–H group in Milstein's catalyst for ester hydrogenation, *Chem. Sci.*, 2021, **12**, 8477–8492.

44 (a) A. Poater, S. V. C. Vummaleti, E. Pump and L. Cavallo, Comparing Ru and Fe-catalyzed olefin metathesis, *Dalton Trans.*, 2014, **43**, 11216–11220; (b) A. Poater, E. Pump, S. V. C. Vummaleti and L. Cavallo, The activation mechanism of Fe-based olefin metathesis catalysts, *Chem. Phys. Lett.*, 2014, **610–611**, 29–32; (c) J. Pecak, R. A. Talmazan, D. Svatunek, K. Kirchner and M. Podewitz, Is Mn(I) More Promising Than Fe(II)? A Comparison of Mn vs Fe Complexes for Olefin Metathesis, *Organometallics*, 2024, **43**, 457–466.

45 (a) H.-J. Knölker, E. Baum, H. Goesmann and R. Klauss, Demetalation of Tricarbonyl(cyclopentadienone)iron Complexes Initiated by a Ligand Exchange Reaction with NaOH-X-Ray Analysis of a Complex with Nearly Square-Planar Coordinated Sodium, *Angew. Chem., Int. Ed.*, 1999, **38**, 2064–2066; (b) A. Pagnoux-Ozherelyeva, N. Pannetier, D. M. Mbaye, S. Gaillard and J.-L. Renaud, Knölker's iron complex: an efficient in situ generated catalyst for reductive amination of alkyl aldehydes and amines, *Angew. Chem., Int. Ed.*, 2012, **51**, 4976–4980; (c) N. Joly, S. Gaillard, A. Poater and J.-L. Renaud, Hydrogen autotransfer with alcohols for alkylations, *Org. Chem. Front.*, 2024, **11**, 7278–

7317; (d) N. Joly, L. Bettoni, S. Gaillard, A. Poater and J.-L. Renaud, Phosphine-free ruthenium complex-catalyzed synthesis of mono- Or dialkylated acyl hydrazides via the borrowing hydrogen strategy, *J. Org. Chem.*, 2021, **86**, 6813–6825.

46 (a) S. Takebayashi, M. A. Iron, M. Feller, O. Rivada-Wheelaghan, G. Leitus, Y. Diskin-Posner, L. J. W. Shimon, R. Avram, L. Carmieli, S. G. Wolf, I. Cohen-Ofri, R. A. Sanguramath, R. Shenhar, M. Eisen and D. Milstein, Iron-Catalysed Ring-Opening Metathesis Polymerization of Olefins and Mechanistic Studies, *Nat. Catal.*, 2022, **5**, 494–502; (b) D. S. Belov, L. Mathivathanan, M. J. Beazley, W. B. Martin and K. V. Bakhryakov, Stereospecific Ring-Opening Metathesis Polymerization of Norbornene Catalyzed by Iron Complexes, *Angew. Chem.*, 2021, **133**, 2970–2974.

